AD-7/GBAR status report for the 2025 CERN SPSC

February 3, 2025

P. Adrich[1], I. Belosevic[2], P. Blumer[3], M. Chung[4], P. Cladé[5], P. Comini[2], P. Crivelli[3], P. Debu[2], A. Douillet[5,6], D. Drapier[5], S. Geffroy[7], S. Guellati[5], P. Guichard[8], P.-A. Hervieux[8], L. Hilico[5,6], P. Indelicato[5], S. Jonsell[9], J-P. Karr[5,6], B. Kim[10], S. Kim[11], E-S. Kim[12], L. Koller[3], N. Kuroda[13], B. Lee[11], L. Liszkay[2], D. Lunney[7], G. Manfredi[8], B. Mansoulié[2], M. Matusiak[1], V. Nesvizhevsky[14], F. Nez[5], B. Ohayon[3], K. Park[11], N. Paul[5], E. Perez[15], P. Pérez[2], J. B. de Queiroz[15], C. Regenfus[3], A. A. Rodríguez Miranda[15], E. Rosin[15], C. Roumegou[7], J-Y. Roussé[2], M. Salman[5,6], F. Schmidt-Kaler[16], K. Szymczyk[1], T. Tanaka[13], B. Tuchming[2], D.-P. van der Werf[17] D. Won[11], S. Wronka[1], P. Yzombard[5],

[1] *National Centre for Nuclear Research (NCBJ), ul. Andrzeja Soltana 7, 05-400 Otwock, Swierk, Poland*
[2] *IRFU, CEA, Université Paris-Saclay, F-91191 Gif-sur-Yvette, France*
[3] *Institute for Particle Physics and Astrophysics, ETH Zurich, 8093 Zurich, Switzerland*
[4] *The Pohang University of Science and Technology (POSTECH), Pohang, Gyeongbuk province, Chungam-Ro77 Hyoja-Dong, Nam-Gu, Pohang, Kyungbuk, 37673, Republic of Korea*
[5] *Laboratoire Kastler Brossel, Sorbonne Université, CNRS, ENS-Université PSL, Collège de France, Campus Pierre et Marie Curie, 4, place Jussieu, F-75005 Paris, France*
[6] *Université d'Evry-Val d'Essonne, Université Paris-Saclay, Boulevard François Mitterand, F-91000 Evry, France*
[7] *Université Paris-Saclay, CNRS/IN2P3, IJCLab, Orsay, France*
[8] *Université de Strasbourg, CNRS, Institut de Physique et Chimie des Matériaux de Strasbourg, UMR 7504, F-67000 Strasbourg, France*
[9] *Department of Physics, Stockholm University, SE-10691 Stockholm, Sweden*
[10] *Center for Underground Physics, Institute for Basic Science, 70 Yuseong-daero 1689-gil, Yuseong-gu, Daejeon 34047, Korea*
[11] *Department of Physics and Astronomy, Seoul National University, 1 Gwanak-Ro, Gwanak-gu, Seoul 08826, Korea*
[12] *Department of Accelerator Science, Korea University Sejong Campus, Sejong-ro 2511, 0019 Sejong, Republic of Korea*
[13] *Institute of Physics, University of Tokyo, 3-8-1 Komaba, Meguro, Tokyo 153-8902, Japan*
[14] *Institut Max von Laue - Paul Langevin (ILL), 71 avenue des Martyrs, Grenoble, France, F-38042*
[15] *CERN, Esplanade des Particules 1, 1217 Meyrin, Switzerland*
[16] *QUANTUM, Institut für Physik, Johannes Gutenberg Universität, D-55128 Mainz, Germany*
[17] *Department of Physics, Faculty of Science and Engineering, Swansea University, Swansea SA2 8PP, United Kingdom*

CERN-SPSC-2025-005 / SPSC-SR-360
03/02/2025

Abstract

We report on the activities performed during 2024 and the plans for 2025 for the GBAR experiment. Highlights include record positron accumulation and an order-of-magnitude increase in antihydrogen production, with several publications in preparation.

1 Introduction

The focus for the 2024 run was to measure the antihydrogen production cross-section using the charge exchange reaction between antiprotons and positronium (Ps):

$$\overline{\mathrm{p}} + \mathrm{Ps} \rightarrow \overline{\mathrm{H}} + \mathrm{e}^- \tag{1}$$

where $\overline{\mathrm{p}}$ stands for antiproton and $\overline{\mathrm{H}}$ for antihydrogen. A schematic diagram of the GBAR experiment is shown in Fig. 1.

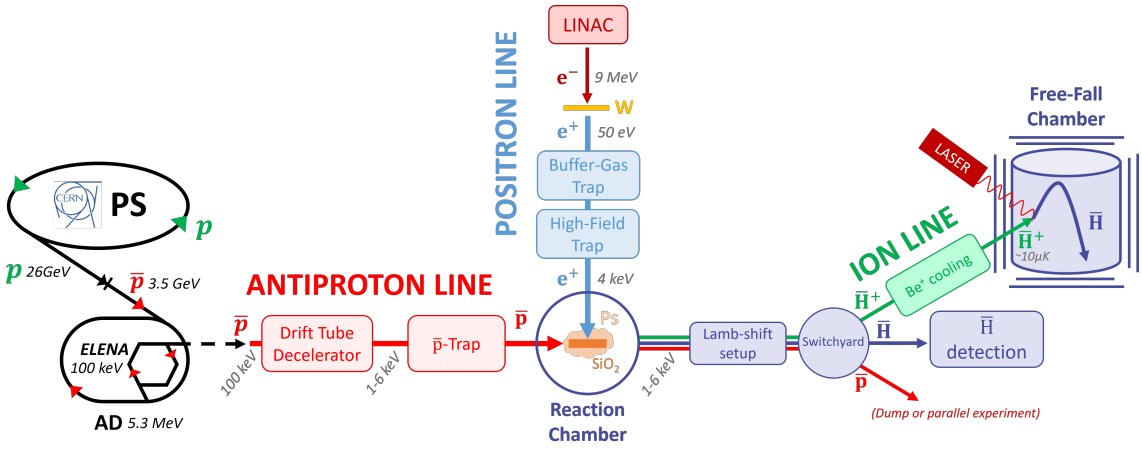

Figure 1: *Schematic view of the GBAR experiment.*

After the publication in 2023 of this production scheme [1], we made several major improvements to the apparatus, including modification of the positronium-target geometry and the integration of a Penning trap for the accumulation and cooling of the antiproton beam. This significantly increased the number of accumulated positrons and antiprotons as well as the antihydrogen-production rate, which allowed accumulating data for the production cross-section at 4 and 6 keV, as well as a more detailed study of the conditions for a measurement of the Lamb shift. Another activity was the preparation of a measurement of the cross-section to produce H^- ions by charge exchange between hydrogen atoms and positronium:

$$\mathrm{H} + \mathrm{Ps} \rightarrow \mathrm{H}^- + \mathrm{e}^+ \tag{2}$$

where the H beam results from the photo-neutralisation of the H^- beam provided by ELENA. In this way we can study with high statistics the matter counterpart of the reaction:

$$\overline{\mathrm{H}} + \mathrm{Ps} \rightarrow \overline{\mathrm{H}}^+ + \mathrm{e}^- \tag{3}$$

to produce anti-ions, since the intensity of the H beam is much higher than that of the $\overline{\mathrm{H}}$ beam.

2 Positron beam line and positronium target

The 9 MeV electrons from the linac bombard a water-cooled tungsten target to produce positrons, which are moderated in a set of annealed tungsten meshes. Recurrent tripping of the accelerator was caused by sparks in the klystron, which was replaced twice during 2024. Tests showed that the klystrons have a deteriorated electron gun, forcing us to use a conservative setting, well below the nominal mean power. As positronium production was limited by the transport between the high-field trap and the target cavity, the lower primary positron beam intensity did not result in a lower antihydrogen production rate. The insulation oil around the klystron was found to have significantly deteriorated insulation properties (a low breakdown voltage) and will be exchanged. For the period until LS3 we will continue working with the available klystrons and will consider repairing one of them.

The silicon carbide remoderator-based trapping scheme in the buffer gas trap [2] proved to be stable and reliable. Further optimization of the trapping sequence significantly improved the efficiency. We could accumulate more than 7×10^9 positrons in the high field trap in about 30 minutes, which is higher than the record value reported by ATRAP (4×10^9 in 4.5 hours [3]). More than 6×10^8 positrons were collected between consecutive antiproton pulses.

The main challenge in producing more positronium lies in transporting positrons between the high-field trap and the positronium target cavity. As the number of positrons increases, space-charge effects become more pronounced and both the plasma dimensions (diameter and/or length) and potential grow. Consequently, moving a larger number of positrons from the 5 T field of the trap to the near-zero field at the target is difficult. To address this issue and increase the number

of positrons delivered to the target, we are presently installing a magnetic field termination grid, composed of thin metallic glass ribbons supported by soft magnetic material, where the beam crosses the magnetic shielding (see Fig. 2). By using high-permeability materials, the grid shortens the transition from the upstream magnetic field of approximately 10 mT to the near-zero field at the target, thus reducing distortions in that region. Simulations of beam transport (using SIMION trajectory analysis and magnetic field maps calculated by COMSOL) demonstrate a significant improvement in transport efficiency, despite losses caused by positron annihilation on the surface.

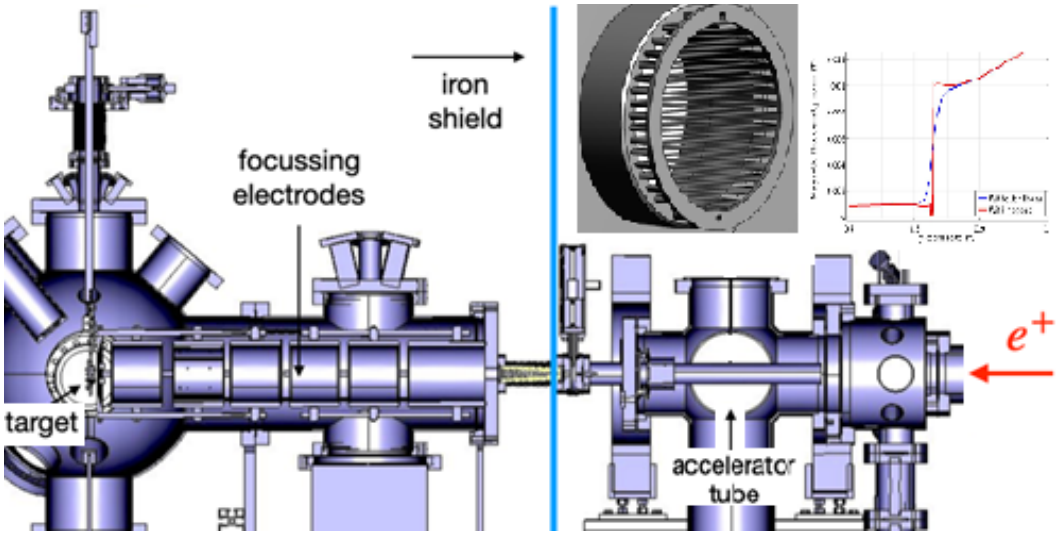

Figure 2: *Schematic view of the positron transport line with the magnetic field termination grid (inset), made of metallic glass ribbons, which will be installed at the entry point of positrons into the magnetic shielding around the reaction chamber (blue line).*

In 2024 we continued to use the positronium target cavity ($2 \times 1.5 \times 20$ mm^3, with a 30 nm Si_3N_4 window) which was successfully commissioned in 2023. The three inner walls of the target are coated with Ps converter material (nanoporous silica). The positron-optics voltages were further optimized to maximise the Ps number, using a Simplex optimisation code. In the production setup 6×10^6 ortho-positronium atoms were produced in the cavity from 3×10^8 positrons ejected from the high-field trap. The Ps fraction is determined by recording SSPALS spectra using a PWO detector placed close to the reaction chamber for targets with and without Ps converter coating. Coupled to a charge measurement on the Ps converter target, the Ps number is then deduced.

3 Antiproton trapping and beam transport

The antiproton trap [4] has been developed to capture the beam from the drift-tube decelerator for cooling before delivery to the reaction-chamber target. Cooling the antiprotons provides better beam emittance (time, spatial and energy spreads) and more flexibility in the handling of the beam from ELENA, such as accumulating several bunches for increased antihydrogen ion production. The antiproton beam line is shown in Fig. 3 where the trap and associated transport optics are indicated.

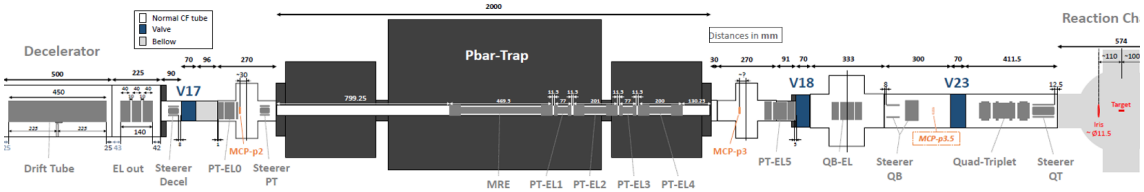

Figure 3: *Schematic diagram of the antiproton line showing the electrostatic optical elements, from the decelerator to the reaction chamber, including the antiproton trap.*

The trap was commissioned during 2023 [2]. Improvements and optimisations were performed

in 2024 to achieve the design parameters as well as routine, stable operation for antihydrogen production data-taking to measure the cross-section. The main improvements concern the trapping efficiency and radial-density profile of the extracted beam.

A trapping efficiency, defined as the ratio of the number of trapped to injected antiprotons (i.e. MCP-p3/MCP-p2 in Fig. 3), of $\epsilon \approx 80\%$ was already achieved in 2023. After electron cooling, the beam is accelerated in a long electrode acting as a drift tube. For each ELENA pulse delivered to the experiment, a beam intensity of about 5×10^6 antiprotons was (routinely) ejected from the trap and sent to the reaction chamber target for mixing. Also, a double-gap buncher was inserted in the acceleration sequence, resulting in a reduced time spread of about 150 ns FWHM.

With the limited beam time after the installation of the trap at the end of last year's run, it was not possible to perfectly align the electric and the magnetic fields. This was improved before the beam time in 2024 by trapping and releasing the H^- beam from ELENA. As a result, the lifetime of the trapped antiprotons was increased from 380 s to 4600 s, as shown in Fig. 4. A short accumulation test resulted in the stacking of more than 10 bunches from ELENA and showed that saturation was not yet reached.

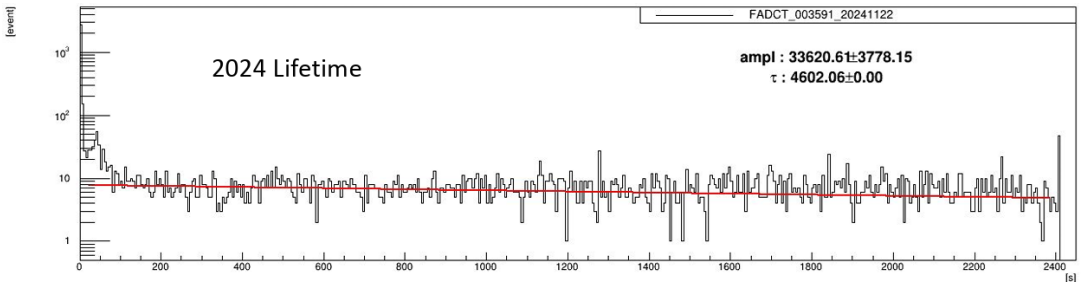

Figure 4: *Count rate in a scintillator detector next to the trap showing long $\overline{p}$ storage time.*

The shape of the potential well in the trapping region is supposed to be harmonic. A first optimisation of the potential shape was performed to increase the plasma density. The parameters of the rotating wall process (frequency and amplitude of the applied wave) were studied, as shown in Fig. 5. The plasma density was improved by about a factor two compared with 2023. Eventually, this translated into the beam transmission efficiency at the reaction target cavity. Because such time-consuming procedures had to be stopped in 2024 to accumulate physics data, they will be one of the major goals during 2025.

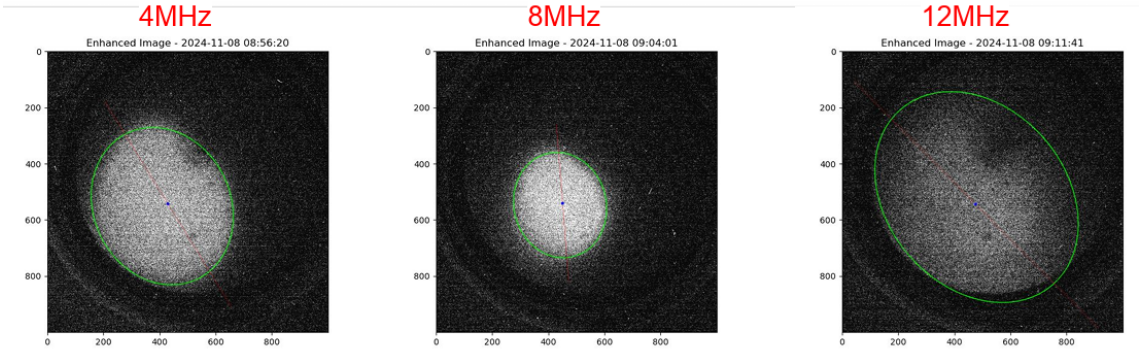

Figure 5: *Extracted antiproton beam shape in MCP at downstream of trap outside of field region for compression by 4MHz (left), 8MHz (middle) and 12MHz (right) rotating wall.*

During the 2024 run a program for the automatic optimisation of the transport of the antiproton beam ejected from the trap was implemented, which saves many days of manual tuning. The voltages of the elements that control the beam line (Fig. 3) are optimised by maximising a user-defined metrics with the Simplex algorithm. The metrics can be computed from signals measured in different detectors. In the simplest case, the metrics is defined by the total signal seen in the detection MCP. Such an optimisation results in a set of voltages that maximises the number of $\overline{H}$ atoms that would be produced in mixing runs. However, this usually results in a beam spot that is not well contained in the MCP, such that large systematic uncertainties on the acceptance would

impede a precise measurement of the $\overline{\mathrm{H}}$ production cross-section. Refining the metrics, using estimators related to the shape of the beam spot and/or annihilation signals seen in upstream scintillators, results in a well-contained, high intensity beam in the MCP. This latter approach has been followed to set up the beam line in view of cross-section measurements. As a result, for each ELENA shot, out of the 5 million antiprotons extracted from the trap at 6 keV, about one million could reach the cavity. Figure 6 (left) shows a typical $\overline{\mathrm{p}}$ beamspot on the MCP with about 10^6 $\overline{\mathrm{p}}$ and a well-contained beamspot. Such a well-contained $\overline{\mathrm{p}}$ beam leads to a well-contained $\overline{\mathrm{H}}$ beam as well, as demonstrated by the cumulative image of all the $\overline{\mathrm{H}}$ candidates from 6 keV cross-section measurement (see Fig. 6 right). Disregarding the requirement that the $\overline{\mathrm{p}}$ beam be well contained in the MCP, the number of $\overline{\mathrm{p}}$ reaching the cavity was nearly twice as large.

The intensity of the antiproton beam delivered by ELENA is monitored for each ejected bunch. The fraction that passes through the positronium target cavity is regularly measured using a CMOS tracker [5] located above the $\overline{\mathrm{H}}$ detection MCP when the electrostatic deflector that is placed right downstream the target is not powered. This device was calibrated when located close to a valve upstream of the $\overline{\mathrm{p}}$ trap receiving the full $\overline{\mathrm{p}}$ beam from ELENA.

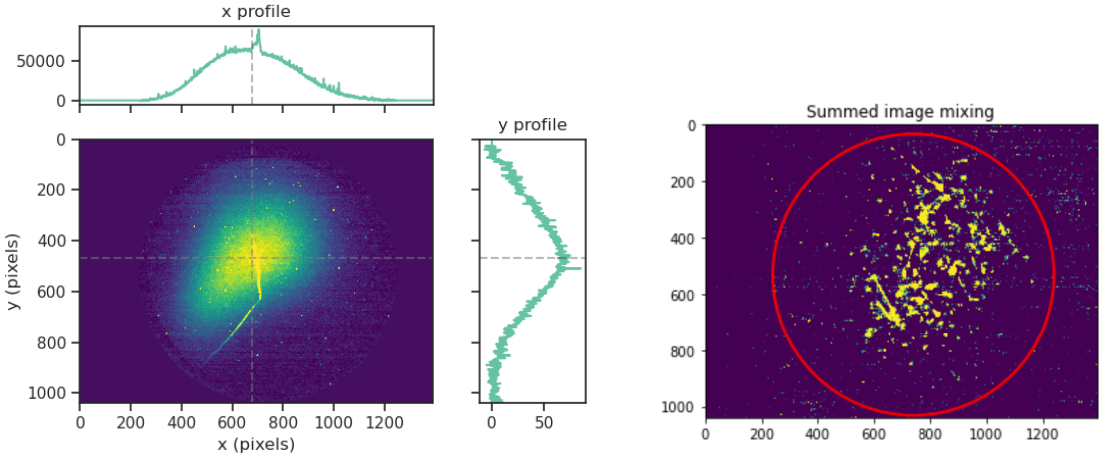

Figure 6: Accumulated MCP images of (left) typical $\overline{\mathrm{p}}$ beam and (right) of synthesized antihydrogen atoms at 6 keV energy

4 GBAR Physics Program

Although we still spend considerable time improving and expanding the apparatus, we now also conduct extensive periods of data accumulation and measurements, as described in the following.

4.1 $\overline{\mathrm{H}}$ production cross-section measurement

In 2023 we published the evidence of $\overline{\mathrm{H}}$ production by the interaction of $\overline{\mathrm{p}}$ from ELENA, decelerated to 6 keV, onto a Ps cloud [1]. However the determination of the cross-section for this process was hampered by the low number of produced $\overline{\mathrm{H}}$ and by a large uncertainty in the acceptance for their detection, resulting in only a lower limit [6]. In the 2024 run, these limitations were addressed through the following improvements:

- The e^+ number is increased as described above (section 2)
- The $\overline{\mathrm{p}}$ bunch from ELENA, decelerated to 3 keV, is trapped and cooled in the $\overline{\mathrm{p}}$ trap before being released with the required energy (e.g. 6 keV or 4 keV) (section 3).
- Care was given to the determination of the number of $\overline{\mathrm{p}}$'s available for the reaction, as explained in section 3.
- Instead of the flat target used to create Ps in 2022, a cavity of $1.5 \times 2\,\mathrm{mm}^2$ section and 2 cm length was used [2]. The use of the cavity instead of the flat target increased the Ps density by roughly a factor of five compared to the 2022 run.

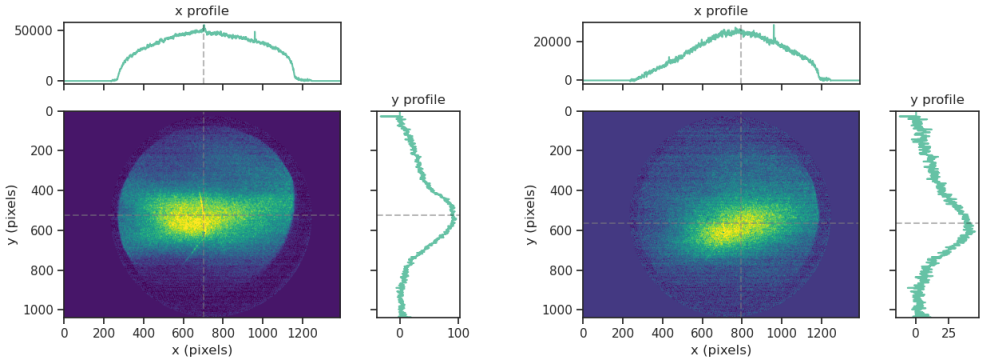

Figure 7: *MCP images of (left) H^- ions and (right) hydrogen atoms created from electron photo-detachment of H^-, downstream of the reaction chamber. The horizontal and vertical beam profiles are also shown. The gray dashed lines indicate the position of the beamspot center, determined by fitting a 2d gaussian to the beamspot.*

- In order to determine the cross-section of reaction (1), the acceptance of both $\overline{\mathrm{p}}$ and $\overline{\mathrm{H}}$ beams must be well understood. The stray magnetic field (0.1-0.5 mT) affects the trajectory of the $\overline{\mathrm{p}}$ beam after the reaction chamber, hence the position of the $\overline{\mathrm{H}}$'s cannot be deduced directly from that of the charged $\overline{\mathrm{p}}$ beam [6]. In order to center the $\overline{\mathrm{H}}$ beam of the mixing runs in the MCP, we use a H beam obtained from the ELENA H^- beam by photo-detachment. A laser pulse is shone on the H^- beam producing neutral H atoms with the same trajectory as that of $\overline{\mathrm{H}}$'s in the measurement configuration. Figure 7 shows the beam profiles in the detection MCP, with the charged H^- and the photo-neutralised H beamspots very close, indicating that the effect of the stray magnetic field is properly compensated. The tuning of the beamline upstream of the reaction chamber is essential.

Preliminary results Details and final numbers will be given in the upcoming publication. Preliminary numbers are given here mainly as a comparison to the 2022 results [1]. For each AD cycle, about 7×10^7 e^+ were delivered to the reaction chamber area, with 2.5×10^7 in the acceptance of the cavity lateral window, producing typically $5 - 6 \times 10^6$ Ps atoms. About 5×10^6 $\overline{\mathrm{p}}$'s were released by the $\overline{\mathrm{p}}$ trap with $0.7 - 1.2 \times 10^6$ in the acceptance of the cavity cross-section for 6 keV $\overline{\mathrm{p}}$ beam. The $\overline{\mathrm{p}}$ bunch length was typically of the order of 150 ns FWHM. In these conditions, the production rate of $\overline{\mathrm{H}}$ atoms at 6 keV is expected to be between 8 and 16 times that of the 2022 run, i.e. between 0.07-0.14 $\overline{\mathrm{H}}$ per AD cycle (depending on the exact run conditions and using the two-center convergent close-coupling cross-section theoretical model [7]). Similar to the 2022 run, "mixing" cycles were recorded with both $\overline{\mathrm{p}}$ and e^+ beams, and "background" cycles with only the $\overline{\mathrm{p}}$ beam present. The numbers are about 3800 mixing cycles and 3400 background cycles recorded with 6 keV incident $\overline{\mathrm{p}}$. About 2000 mixing cycles and 1300 background cycles were recorded with 4 keV incident $\overline{\mathrm{p}}$. Fig. 8 shows an accumulation of the number of detected events on the MCP as a function of the arrival time of $\overline{\mathrm{H}}$ candidates for mixing and background cycles of the 6 keV dataset. The clear surplus of events in the expected time window demonstrates the improvement in the number of detected $\overline{\mathrm{H}}$ atoms by almost a factor of 30 compared to the 2022 dataset and with a better signal-to-noise ratio. We are presently analysing the data and determining the systematic uncertainties with the goal of establishing the cross-section (at 6 keV and 4 keV) for this reaction.

4.2 Antihydrogen Lamb shift

For 6 keV antiprotons around 10 % of the antihydrogen are expected to be formed in the 2S state by the charge exchange reaction with the positronium atoms. This opens up the possibility for precision experiments with a keV-beam of $\overline{\mathrm{H}}$ including a measurement of the Lamb shift (2S to 2P transition) of $\overline{\mathrm{H}}$ atoms with a precision of 100 ppm, which will allow to determine the anti-proton charge radius to 10 % [8].

Upgraded Lamb shift setup and first tests with the H^- beams and the carbon foil The detection system (Fig. 9) is based on 2S to 2P mixing of $\overline{\mathrm{H}}$ atoms via electrical quenching, where the 2P decays to the ground state within a few ns, emitting a Lyman-α photon (121.6 nm). The quenching location is surrounded by CsI-coated MCPs that can efficiently detect the photons,

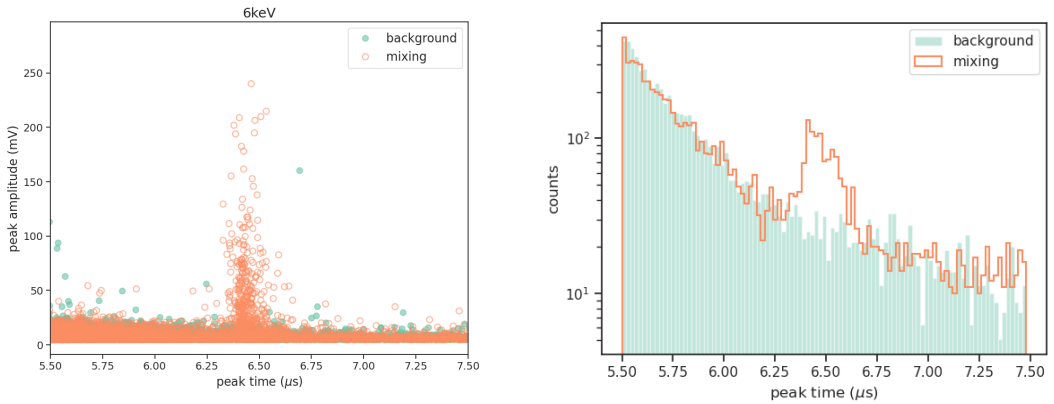

Figure 8: (left) Amplitude vs time of peak MCP signal (right) time-of-flight histogram of antihydrogen-atom pulse heights.

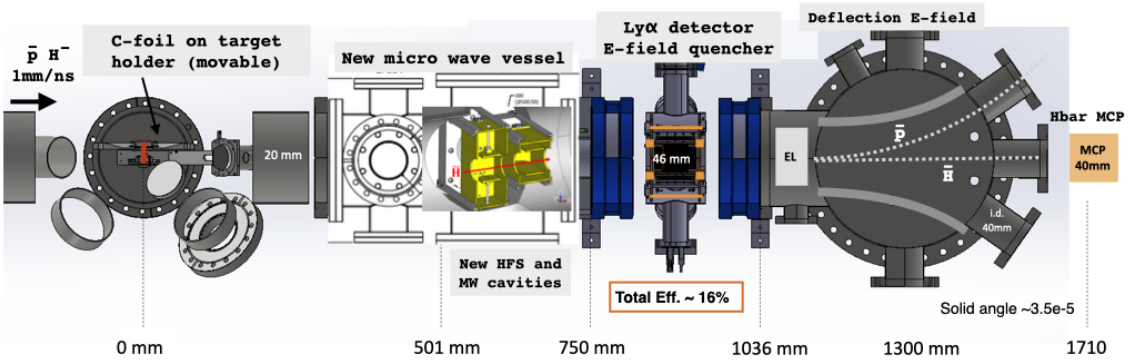

Figure 9: *Arrangement of the Lamb shift components. The* $\overline{\mathrm{p}}$ *or* H^- *beams come from the left into the target area where the oPs cavity or a thin carbon foil can be selected to produce* $\overline{\mathrm{H}}$ *or H. The atoms then pass two MW regions where the HFS state can be selected and the line can be scanned. Surviving 2S states are then quenched by an E-field in the detection volume where the Lyman-α photons from the rapidly decaying 2P states are detected by 4 square MCPs with a CsI coating (deep UV).*

turning the measurement into a simple counting experiment. A microwave setup with two zones for selecting the hyperfine state (HFS) and driving the 2S to 2P transition is placed upstream of the detector. Depending on how far off-resonance the microwave is, hence driving the transition less efficiently, more counts can be seen in the MCPs. The HFS selector will be used at a later stage for a higher precision measurement of the Lamb shift via the 910 MHz transition only, by quenching the other transitions away, as done for hydrogen [9].

The Lyman-α detection system was first successfully commissioned at the low energy muon beam line at PSI under conditions of rates and energies (few keV) close to GBAR, leading to a precise measurement of the muonium Lamb shift [10]. With the experience gained at PSI a 10 nm thin carbon foil was installed in GBAR together with the Lamb shift setup in 2021. Using a proton source the setup was commissioned and first spectra were measured as reported in 2022 [11]. An upgraded setup [12], installed in 2024, includes an optimisation of the microwave spectrometer, now equipped with new MW cavities with 30 mm opening (Fig. 10 left), and of the vacuum chamber to reduce the annihilations of antiprotons that can produce a signal in the Lyman-α detectors (Fig. 9).

In 2024, with the H^- beam from ELENA transported in pass-through mode of the $\overline{\mathrm{p}}$ trap and impinging on the C-foil, about 600 neutral H-atoms per spill could be detected on the $\overline{\mathrm{H}}$ MCP (Fig. 10 middle) As in the case of protons impinging on a thin carbon foil, a fraction of these neutral atoms are produced in the 2S state [13] and can be used to test the Lamb-shift set-up. Lyman-α signals could be detected as indicated by the MW OFF/ON measurements (Fig. 10 right). Unfortunately these measurements show that the efficiency to detect deep-UV photons by the CsI coated

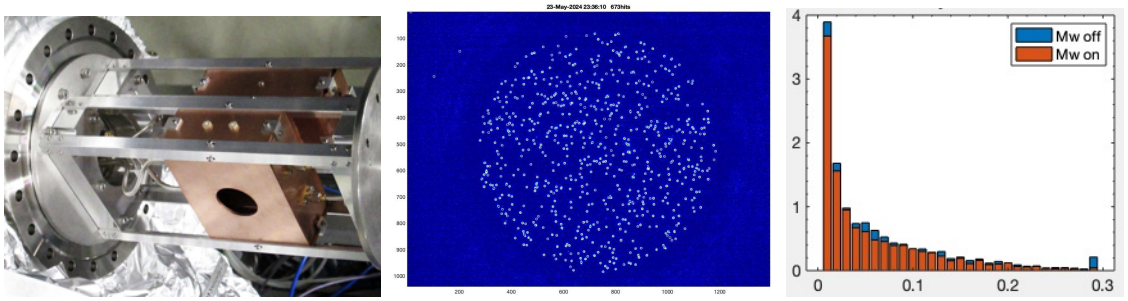

Figure 10: (left) new Lyman-α microwave (MW) cavities. (middle) MCP image of neutral H atoms produced by the H^- beam impinging on the carbon foil. (right) pulse height spectra for MW OFF/ON with a small excess of Lyman-α signals (MW OFF) over the background.

MCPs reduced significantly over the last years. A similar effect was found at PSI and attributed to ageing of the thin evaporated (hygroscopic) CsI layer. The layer will be redone in 2025 in the surface coating lab at CERN.

Testing, characterisation and calibration of the LS setup with the H^- beam. The LS setup will be commissioned with the H^- beam and a two-times thinner C-foil that was tested at PSI for less beam straggling and hence less background. The H^- cycle of ELENA is about a factor of 6 shorter in comparison to $\overline{p}$'s and several tens of H 2S states will be produced per spill. This will give us the best conditions to test and calibrate the entire experimental setup. MW frequency scans will be used to explore the best analysis strategy for achieving the most precise combined line fits to the data. The results will then be compared to data taken with the hyperfine selector (HFS) in operation. In 2025, the goal is to detect the Lyman-α photons from $\overline{H}$ atoms created in the charge exchange reaction in the 2S state. In 2026, after the setup optimisation in the Winter break the first spectroscopic measurements of the Lamb shift will be performed.

4.3 The Study of Positronium-Hydrogen Interactions (SPHINX) project

In 2024, GBAR made significant experimental progress toward the production of $\overline{H}^+$ by demonstrating more than one order of magnitude gain in $\overline{H}$ production and breaking records in positron accumulation. However, there remains an uncertainty on the cross-section of reaction (3). This has never been measured experimentally, and the theoretical calculations differ greatly depending on the models, sometimes by an order of magnitude. Depending on the value of this cross section, GBAR may have to further increase its positron production and trapping performances or revise its $\overline{H}^+$ production scheme.

Principle. Thanks to its intense positron source and to the opportunity offered by the H^- beam provided by ELENA, GBAR has the capacity to measure this cross section for the charge conjugated reaction: $H + Ps \rightarrow H^- + e^+$ for the first time. The whole GBAR set-up as currently installed at CERN is required for the measurement. The positron line is used to prepare a dense ortho-positronium target at a higher repetition rate compared to the usual scheme with antiprotons (over 10^8 accumulated positrons can be sent to the reaction tube every 45 seconds). The ELENA H^- pulsed beam, delivered every 15 seconds, is decelerated to the desired kinetic energy by the GBAR pulsed drift tube and transported to the reaction chamber where it is partially neutralised. This neutralisation part is the main addition of the SPHINX project to the GBAR set-up. It takes place between the last focusing stage before the reaction tube and the reaction tube itself. The H^- beam is illuminated by a pulsed laser over a length of 100 mm. The remaining H^- are electrostatically deflected away for monitoring, while the neutral hydrogen pulse proceeds to the reaction tube for interaction with the positronium. The newly formed H^- ions continue to the switchyard together with the hydrogen beam. There, the charged and neutral hydrogens are separated: the H^- are deflected and focused onto an MCP detector.

Status. In 2024, the design studies for the opto-mechanical components of the SPHINX project were finalised. The optics supports in the reaction chamber (see Fig. 11) and optical bench outside have been produced and will be integrated to the GBAR set-up in February 2025, complementing the already installed optical breadboard and electrostatic deflector, in the reaction chamber, and

the MCP detector.
Owing to the general improvement of the antiproton beam transport in 2024, we decided to reevaluate the possibility to use the H^- beam in pass-through mode with the antiproton trap. We used the extra week of H^- beam allocated to GBAR to perform this critical test. After optimisation, we measured that only 3 % of the H^- ELENA beam is transmitted through the reaction tube when transported through the $\overline{p}$ trap, while from 2022 tests and SIMION simulations, we expect three to five times more using the former transfer line without the trap. Assuming at least a fractor three improvement in the H^- transport efficiency, the expected signal-detection rate is between 3×10^{-3} and 3.5×10^{-2} per shot, depending on the theoretical cross section model. [14, 15] At 6 keV the background coming from electron capture by neutral H on the residual gas is estimated to be at most 1.7×10^{-3} at 10^{-10} mbar. [16]

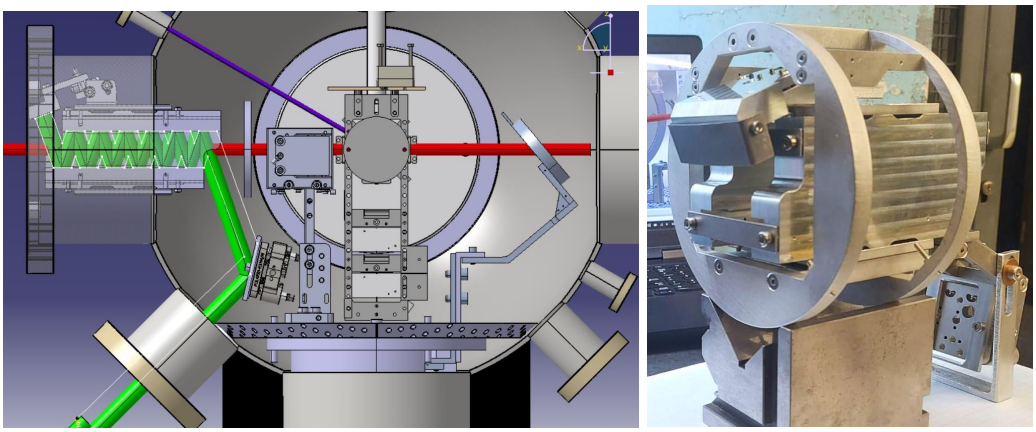

Figure 11: *(left) CAD drawing of the SPHINX photodetachment section inside the reaction chamber with (right) a photograph of the realisation. The H^- ions (red beam) come from the left and pass between two mirrors within which the laser (green beam) neutralises part of the beam upstream of the deflector and reaction cavity on the target holder.*

Plans for 2025. The antiproton trap will be replaced with the transfer line for the SPHINX measurements in early 2025 while the $\overline{p}$ trap will undergo upgrades and work off-line with electrons in the meantime. The first two months of H^- beam will be dedicated to the commissioning of the SPHINX set-up and a first measurement of the background. This will be followed by two months of data taking with ELENA providing the H^- beam only during day time on week days. The primary goal in 2025 is to provide a cross section value with a precision better than 50 % at 6 keV hydrogen kinetic energy and for ground state positronium. Other beam energies may be investigated in parallel with GBAR's antiproton program. In this perspective, a possibility to measure antihydrogen production cross section at energies not accessible with the antiproton trap is considered to make the most efficient use of the beamtime during spring 2025.

5 Activities in Collaborating Institutes

Several collaborators are working in their laboratories outside CERN. A dedicated on-line meeting took place on October 16, 2024 to review these activities.

At Université Paris-Sorbonne, LKB collaborators are working on the following topics :
• Improved calculations of the H^- binding energy: Including relativistic and QED corrections to reach the 0.1 µeV accuracy level will allow to precisely know the photodetachment laser frequency detuning with respect to the photodetachment threshold, a key data to determine the resulting H recoil.
• Measurement of H^- photodetachment threshold. Photodetachment laser characteristics relevant to the experiment have been precisely evaluated and a laser solution proposed.
• $\overline{H}^+$ stripping probability during sympathetic cooling: Sympathetic cooling of the $\overline{H}^+$ ion takes place during hundred thousands round trips in a laser cooled Be^+ ion cloud during which Coulomb interaction with the Be^+ ions may detach the $\overline{H}^+$ excess positron. A detailed numerical simulation of the detachment process along trajectories confirms that $\overline{H}^+$ ions survive the cooling process.
• Sympathetic cooling experimental simulation in GBAR proxy: $\overline{H}^+$cooling by a Be^+ ion cloud is

experimentally simulated on the $Be^+ + Sr^+$ cooling platform in collaboration between LKB and MPQ laboratories. A two-trapping zone surface ion trap was used and successful launching of Sr^+ ions from one zone to the other with a controlled kinetic energy was presented [17].
• Precise magnetometers: 12 magneto-resistive sensors, with mG sensitivity and a range of ± 30G have been installed in June-July 2024, with the help of a CERN summer student. These sensors have been mainly installed inside the magnetic shielding around the reaction chamber, in order to diagnose the variations of the B field and try to correlate to the optimization of the steering of the positrons toward the reaction chamber.

Theoretical developments are being pursued at the IPCMS Strasbourg to explore different anti-atomic processes accessible to the GBAR set-up, in particular the formation of antihydrogen molecular ions, the formation of positronium hydride and positronium-positronium collisions. In addition, numerical simulations of electron cooling of positron beams have been developed.

6 Outlook

After a first successful increase of the $\overline{H}$ production rate, we aim at extending the energy range of our cross-section measurements for reaction 1 as well as making a first measurement of the cross-section of reaction 2. In parallel, efforts will focus on improving beam transport to the reaction target to allow first measurements relative to the Lamb shift and progress toward $\overline{H}^+$ production.

7 Requests

In addition to the antiproton beam, the H^- beam provided by ELENA is a valuable tool for GBAR. However, the steering of the H^- beam is a tedious task due to the AD magnetic field variations during the antiproton cooling cycle. We will use the H^- beamtime in March before the restart of the AD to speed up H^- steering. In order to use more efficiently the H^- bunches provided between antiproton ejections after the AD restart, we would like to request the implementation of a beam displacement compensation in the LNE50 beamline to ensure that the H^- beam remains well aligned in our drift tube.

We would also benefit from faster access to the ELENA data for our beam-transport optimisation program, which would be more efficient if we could correct in real-time for the beam intensity fluctuations. The issue is particularly important for the H^- beam intensity, which can fluctuate by a factor two, while we observed that the update of the ELENA data on TIMBER can take more than the 15 s between two pulses.

Finally, we support the exploration of another H^- functioning mode in ELENA which would not require to cycle the ELENA magnets: this would allow GBAR to take H^- beam during the YETS periods while minimising the impact on the BASE experiment.

8 Acknowledgments

We thank F. Butin and the CERN EN team, L. Ponce and the AD/ELENA team for their fruitful collaboration. The ELENA H^- beam has proven to be an excellent tool to check beam alignment and to commission detectors in GBAR. It can be used for physics measurements such as the one promoted by the SPHINX project. We want to thank the BE department and the ELENA team for the provision of the H^- beam and we strongly support its consolidation.

References

[1] P. Adrich et al. Production of antihydrogen atoms by 6 keV antiprotons through a positronium cloud. *Eur. Phys. J. C*, 83(11):1004, 2023. [Erratum: Eur.Phys.J.C 83, 1069 (2023), Erratum: Eur.Phys.J.C 84, 1143 (2024)].

[2] The GBAR Collaboration. AD-7/GBAR status report for the 2024 SPSC, https://cds.cern.ch/record/2888058.

[3] D W Fitzakerley, M C George, E A Hessels, T D G Skinner, C H Storry, M Weel, G Gabrielse, C D Hamley, N Jones, K Marable, E Tardiff, D Grzonka, W Oelert, M Zielinski, and (ATRAP Collaboration). Electron-cooled accumulation of 4×10^9 positrons for production and storage of antihydrogen atoms. *Journal of Physics B: Atomic, Molecular and Optical Physics*, 49(6):064001, 2016.

[4] Kyoung-Hun Yoo et al. Design study of an antiproton trap for the GBAR experiment. *JINST*, 17(10):T10003, 2022.

[5] The GBAR Collaboration. AD-7/GBAR status report for the 2023 SPSC, https://cds.cern.ch/record/2848094.

[6] Corentin Roumegou. *Synthesis of antihydrogen from in-flight charge exchange of decelerated antiprotons in positronium for the GBAR experiment.* PhD thesis, Université Paris-Saclay, 2023, https://cds.cern.ch/record/2883050.

[7] C. M. Rawlins et al. Calculation of antihydrogen formation via antiproton scattering with excited positronium. *Phys. Rev. A*, 93:012709, 2016.

[8] P. Crivelli, D. Cooke, and M. W. Heiss. Antiproton charge radius. *Phys. Rev. D*, 94(5):052008, 2016.

[9] N. Bezginov, T. Valdez, M. Horbatsch, A. Marsman, A. C. Vutha, and E. A. Hessels. A measurement of the atomic hydrogen lamb shift and the proton charge radius. *Science*, 365(6457):1007–1012, 2019.

[10] B. Ohayon et al. Precision Measurement of the Lamb Shift in Muonium. *Phys. Rev. Lett.*, 128(1):011802, 2022.

[11] P Pérez. AD-7/GBAR status report for the 2022 CERN SPSC. Technical report, CERN, Geneva, 2022.

[12] T. A. Tanaka et al. Design of a microwave spectrometer for high-precision lamb shift spectroscopy of antihydrogen atoms. *Hyperfine Interact.*, 245(1):30, 2024.

[13] Frédéric Allegrini, Robby Ebert, Stephen Anthony Fuselier, Georgios Nicolaou, Peter V. Bedworth, Steven W. Sinton, and Karlheinz J. Trattner. Charge state of 1 to 50 kev ions after passing through graphene and ultrathin carbon foils. *Optical Engineering*, 53, 2014.

[14] P Comini, P-A Hervieux, and K Lévêque-Simon. Corrigendum: $\bar{H}^+$ ion production from collisions between antiprotons and excited positronium: cross sections calculations in the framework of the gbar experiment (2013 New J. Phys. 15 095022). *New Journal of Physics*, 23(2):029501, 2021.

[15] Takuma Yamashita, Yasushi Kino, Emiko Hiyama, Svante Jonsell, and Piotr Froelich. Near-threshold behavior of positronium-antihydrogen scattering cross sections. *Phys. Rev. A*, 105:052812, 2022.

[16] B. Van Zyl, T. Q. Le, and R. C. Amme. Charged-particle production in low-energy $H+H_2$ and H+He collisions. *The Journal of Chemical Physics*, 74(1):314–323, 1981.

[17] Derwell Drapier. *Sympathetic Cooling of a Be^+ Ion by a Sr^+ Coulomb Crystal: A Testbed for Taming Antimatter Ions.* PhD thesis, Université Paris-Sorbonne, 2024. https://www.lkb.fr/iontrap/wp-content/uploads/sites/15/2025/01/Derwel_Drapier_comp.pdf.